

NUMERICAL SIMULATION OF THE SYMMETRIC LASER-SHOCK BASED DISASSEMBLY PROCESS FOR ADHESIVELY BONDED TI/CFRP PARTS

**PANAGIOTIS KORMPOS^{*}, KONSTANTINOS TSERPES^{*}, SELEN UNALDI[†],
LAURENT BERTHE[†]**

^{*}Laboratory of Technology & Strength of Materials (LTSM), Department of Mechanical
Engineering & Aeronautics, University of Patras, Patras 26504, Greece.

e-mail: kitserpes@upatras.gr

[†]PIMM, UMR8006 ENSAM, CNRS, CNAM, 151 bd de l'Hôpital, 75013 Paris, France

Abstract. Novel engine fan blades are made from 3D woven composite materials and incorporate a protective metallic layer at the leading edge. The end-of-life of such structures involves complicated disassembly and recycling processes. Laser-shock is being investigated as an environmentally friendly disassembly method. In this context, symmetric laser-shock experiments that were conducted in a previous work using a time delay between the shots have been proven successful for debonding initiation and propagation. In this paper, a numerical model simulating the symmetric laser-shock disassembly of Ti/CFRP specimens has been developed using the LS-Dyna explicit FE code. The objective of the model is to give a deeper insight of the physical mechanisms and to optimize the experimental process. To obtain input for the composite damage model, Split-Hopkinson tests have been conducted. The numerical results correlate well with back-face velocity profiles, experimentally obtained by VISAR measurements, and damage patterns in the adhesive and the composite material, experimentally characterized by electronic microscope photographs.

Key words: Disassembly, Laser-shock, Dynamic testing, Numerical simulation, Finite element analysis

1 INTRODUCTION

In the aerospace industry, end-of-life aircraft recycling presents significant sustainability challenges, and a variety of disassembly strategies exist for aircraft and engine end-of-life solutions [1], although they usually do not account for adhesively bonded joints.

Adhesive bonding has become increasingly popular in the manufacturing industry due to its numerous advantages, such as reduced weight, and improved load transfer capabilities. However, these adhesive joints present a significant challenge during end-of-life disposal and recycling, as they are difficult to separate without causing damage to the components [2]. This creates a need for disassembly of adhesively bonded structures in a sustainable and efficient manner. The disassembly of adhesively bonded structures constitutes a crucial stage in the recycling and disposal of such materials. Debonding techniques currently utilize high temperatures and mechanical forces in order to separate the adherants. This approach, while it is easy to implement, removes the re-use option of the structure as it causes thermal and mechanical damage to the involved materials [3]. Current research addresses this challenge by developing bonded joints that facilitate disassembly, by employing debonding on demand

solutions, such as thermally expandable particles [4-5]. However, their use as structural components is currently limited due to their inferior mechanical properties [5].

The present study examines the laser-shock process as a disassembly technique. The innovation of the laser-shock disassembly process lies in its precision of load application, which restricts damage at the bondline or interface, provided the laser parameters have been adequately calibrated [6]. To study this technique, it is applied to a multi-material specimen consisting of 3D woven CFRP that incorporates a metallic protective edge, which is a novel assembly for an engine fan blade.

The laser-shock technique involves the interaction between a high-powered laser and a target material, which creates a plasma expansion that induces pulsed pressure through the recoil momentum of the ablated material. The plasma expansion generates an elastic precursor shock followed by an elastic-plastic compression shock that propagates through the material. After the plasma expansion, the surface unloads, and a plastic-decompression shock alongside an elastic-plastic decompression shock starts to propagate, creating a release wave. When the release wave interacts with the elastic precursor shock wave, it creates high localized tensile stresses. The most cost-effective way to optimize a complex experimental procedure is to simulate the process and numerous simulation studies have been conducted to investigate and characterize the laser-shock phenomenon [7-10]. This study aims to create an accurate model of the specimen that is used in experimental work, using LS-Dyna FE explicit code.

First, the experimental procedure of the laser-shock based disassembly is being described, then Split Hopkinson experiments are detailed and the results are presented. The model and simulation techniques are explained alongside the FE models, and finally the results of the simulations are showcased.

2 EXPERIMENTAL

2.1 Laser shock experiments

Different setups can be created based on the configuration of the two beams. Figure 1(a) shows the standard single-sided shot configuration and figure 1(b) illustrates the symmetric configuration achieved using two polarized beams separated by a 90° polarizer and transported to each side of the specimen using optics.

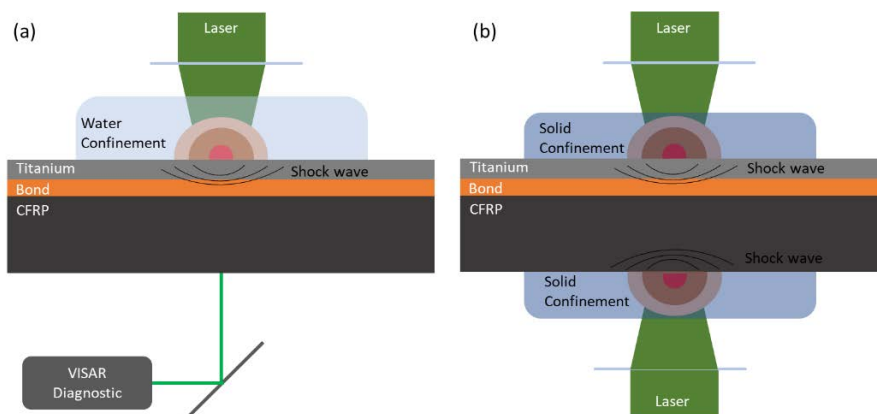


Figure 1: Laser-shock experimental set-ups. Single-sided shot with back-face velocity measurements (a) and symmetric shot (b)

Experiments utilizing both setups have been conducted and in depth description alongside the produced outputs has been detailed in a previous work [6]. Briefly, the single sided setup consists of shots at the surface of the specimen utilizing water as the confinement regime, while at the backface an optical diagnostic tool (VISAR) is measuring the particle velocity. Back face velocity measurements are essential for the validation of the numerical model as described in section 4.4. The symmetric experimental setup is critical for the achievement of the debonding between the Ti and CFRP. By utilizing the symmetric technique, the maximum tensile stress can be shifted to different locations by applying a time delay (Δt) between the pulses. The maximum tensile stress is produced by the interference of the two reflected release waves, and its position at the material's thickness depends on Δt . The achieved debonding is then used for the validation of the simulation of the interface between Ti and CFRP.

2.2 Split Hopkinson experiments

The dynamic behavior of a material is different from the static one because of inertia effect and the propagation of stress waves. To simulate the laser-shock process, the composite material model that is described in section 4.2 requires material properties measured in high strain rates. In that context, to characterize the composite material under high strain rate, the Split-Hopkinson pressure bar apparatus (SHPB) was used. Stress – Strain curves at high strain rates can be acquired from the stress waves propagating through the incident and the transmitted bar in the apparatus. The strain rate that can be achieved is in the range of 1000/s to 10000/s depending on the specimen type. The basic design of the split Hopkinson pressure bar has been modified for high strain rate tensile [11] and punch shear testing [12].

Figure 2 illustrates the principle of the Split Hopkinson Pressure Bar (SHPB). A striker bar is propelled by a gas gun and collides with the incident bar, which generates a pulse that propagates into the specimen. A compressive pulse is transmitted through the specimen to the transmitted bar, while the remainder of the pulse is reflected into the incident bar as a tensile pulse. In the case of a tensile SHPB illustrated in figure 2 (b), the tensile and compressive pulses appear on the transmitted and incident bars, respectively. Strain gauges are positioned equidistantly from the specimen to measure both the transmitted and reflected pulses.

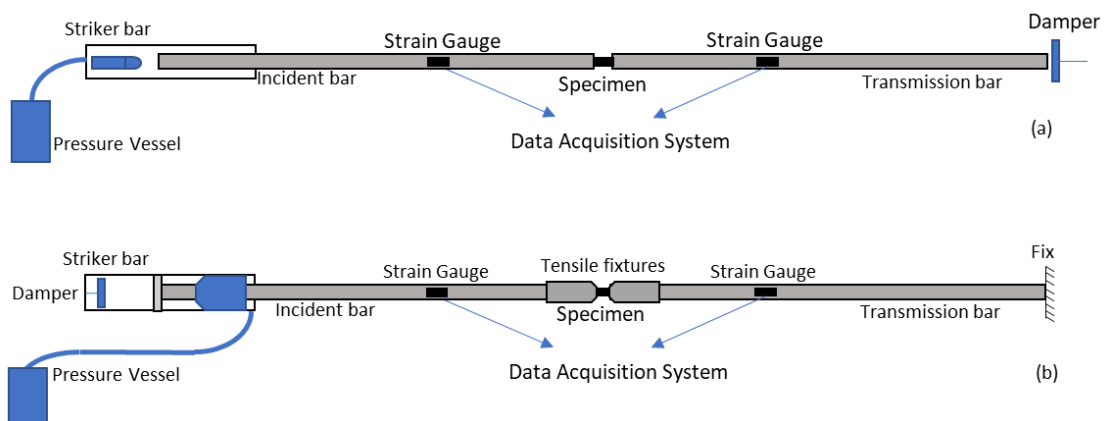


Figure 2: Schematic representation of the compressive (a) and tensile (b) SHPB apparatus

The specimens were cut from a single plate of 3D-woven CFRP with thickness of 5.45 mm. The dimensions for the tensile and punch shear specimens are 100×20 mm and 40×40 mm respectively. Figure 3 illustrates the specimens.

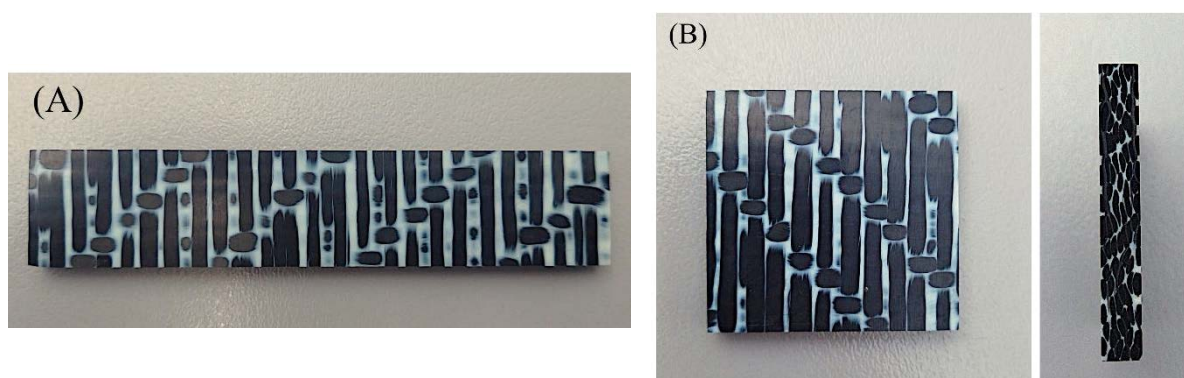


Figure 3: Tensile specimen (a) and punch shear specimen (b)

2.2.1 Tensile testing

Tensile tests were conducted on specimens extracted from a single plate with orientations of 0° (weft) and 90° (warp). To secure the specimens to the grips, emery cloth was utilized, and the clamping force was controlled using a torque wrench set to 75 Nm. Two sets of antipodally positioned strain gauges were employed for data acquisition, to account for potential bending during the experiments. For measurement acquisition, storage, and processing, a LabVIEW environment was developed, allowing for the selection of sampling rates. For tensile testing, the sampling rate was set to 2 MHz. The experiment was controlled by the pressure of the gas gun, ranging from 1 to 6 bars, with the pressure set to 4.1 bars for the tensile experiments. Higher pressure led to sample slippage, rendering it impractical to use for the given specimen thickness. As a result, only elastic properties were obtained from the 0° specimen, whereas the 90° specimen was tested until failure using 4.1 bars of pressure, resulting in the complete stress-strain curve.

2.2.2 Punch shear testing

In order to achieve shear loading in the Split Hopkinson Pressure Bar (SHPB) apparatus, modifications were made to the compressive part. A fixture was designed and constructed specifically for this purpose [12]. Similar to the standard methodology employed in compressive split Hopkinson testing, the specimen was secured between the fixture using petroleum jelly to hold it in place, and to reduce friction during loading. To determine the actual contact area for stress and strain calculations, a high-speed camera was utilized to observe the experiment. Data acquisition was performed using strain gauges placed at an equal distance from the specimen on both the incident and transmitted bars, with two strain gauges used at each bar to account for potential bending during the experiment.

The strain and stress equations were modified using the asymmetric surface contact areas present in the punch shear fixture.

2.3 Split Hopkinson experimental results

Regarding the tensile experiments, in the case of specimens that were cut following the wrap orientation, failure was not observed during the experiments. Consequently, only elastic properties could be extracted from the results. In contrast, the specimens that were cut following the weft orientation, failed and, thus, the full stress-strain curve was obtained. Figure 4 contains the stress-strain curves for the tensile experiments, while table 1 presents the resulting properties.

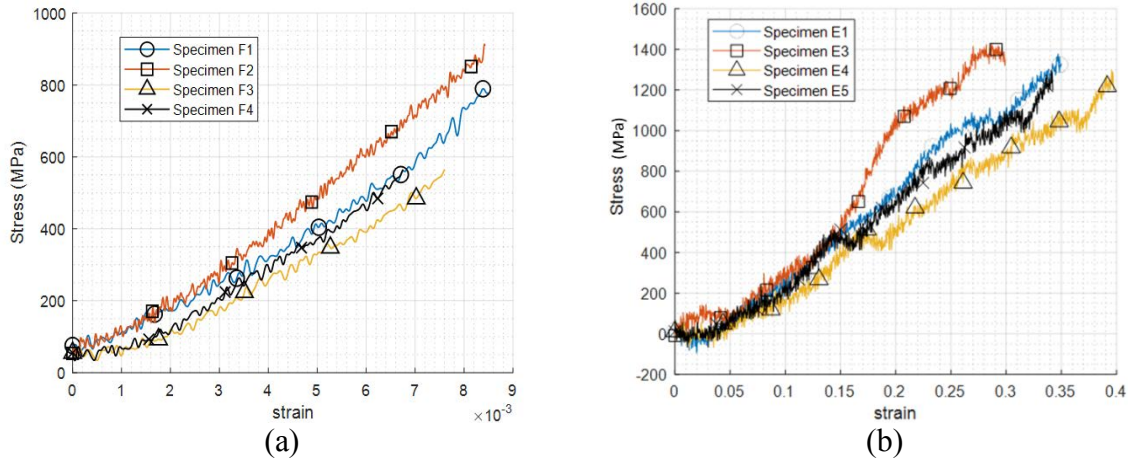


Figure 4: Stress-strain curve for the warp (a) and weft (b) orientation specimens

Table 1: High strain rate tensile properties for the 3D woven composite

Property	Wrap	Weft
Max strain rate	50 /s	900 /s
Elastic Modulus	80.27 GPa	4.17 GPa
Elastic Modulus dev.	6 GPa	0.286 GPa
Max Stress	No failure	1342 MPa
Max Stress dev.	No failure	70.66 MPa

Regarding the punch shear testing, it is worth noting that all specimens failed during the experiments. The shear properties that were obtained from these experiments are presented in Table 2.

Table 2: High strain rate shear properties for the 3D woven composite

Property	Perpendicular to fibers	Parallel to fibers
Max strain rate	10000 /s	10000 /s
Shear Modulus	3.69 GPa	2.94 GPa
Shear Modulus dev.	0.26 GPa	0.7 GPa
Max Stress	1240 MPa	963 MPa
Max Stress dev.	166 MPa	174 MPa

3 NUMERICAL MODEL

3.1 Specimen and materials

The specimen that is modeled is made by a 3D- woven CFRP core bonded to a thin Ti alloy edge using an adhesive film. Each specimen was cut from a single block and the final dimensions of the specimens are 100 mm × 40 mm with a thickness of 10.6 mm.

3.2 Laser-shock loading application

The ablation pressure used in the simulations is described by figure 5 and the maximum pressure Pmax (GPa) is calculated by Eq.1 [13]

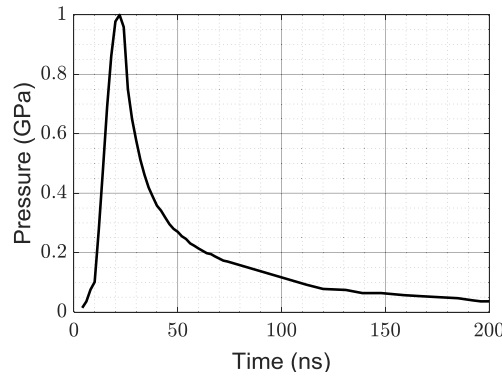


Figure 5: Normalized pressure temporal profile

$$0.01 \sqrt{\frac{\alpha}{2\alpha + 3}} \sqrt{Z I_0} \quad (1)$$

$$Z = 2 \frac{Z_1 Z_2}{Z_1 + Z_2} \quad (2)$$

Where I_0 (GW/cm²) is the Laser's intensity, α is the part of the energy being used for the ionization and Z (g cm-2/s-1) is the relative acoustic impedance where Z_1 and Z_2 are the acoustic impedance of the material and confinement respectively.

3.3 Material models

3.3.1 Johnson-Cook material model

To simulate the high strain rate behavior of the titanium due to the shock wave loading, the Johnson–Cook plasticity model [14] and the Grüneisen equation of state [14] were used. Thermal effects have not been simulated. The flow-stress expression of the material model is

$$\sigma_y = \left(A + B \bar{\epsilon}^{p^n} \right) \left(1 + c \ln \dot{\epsilon}^* \right) \left(1 - T^{*m} \right) \quad (3)$$

where $\bar{\varepsilon}^p$ is the effective plastic strain, $\dot{\varepsilon}^*$ the normalized effective total strain-rate (for VP.EQ. = 0), m the thermal softening and T^* is the homologous temperature. Strain at fracture is calculated by

$$\varepsilon^f = (D_1 + D_2 e^{D_3 \sigma^*}) (1 + D_4 \ln \dot{\varepsilon}^*) (1 + D_5 T^*) \quad (4)$$

where s^* is the ratio of pressure divided by the effective stress.

Titanium is a well-studied material for high strain rate applications and properties for the Johnson-Cook material model and the Grüneisen equation of state have been derived from literature [15], [16].

3.3.2 Composite progressive damage material model

The present investigation employs MAT_162 for the analysis of 3D woven composite materials. This model is characterized by strain rate dependent constants and a progressive damage formulation. Both unidirectional and woven composite configurations can be applied within the framework of this constitutive model. To describe the failure mechanisms of composite materials, a variety of failure criteria can be incorporated into the MAT_162 formulation. Specifically, the model can simulate fiber failure, matrix damage, and delamination phenomena under various loading scenarios, including opening, closure, and sliding modes of failure. The degradation of material properties is accounted for through the use of a damage parameter ω_i within the stiffness matrix, which controls the progressive reduction in material strength and stiffness. The growth rate of damage variable, $\dot{\omega}_i$, is controlled by the damage rule of the form:

$$\dot{\omega}_i = \max\{\Phi_j q_{ij}\} \quad (5)$$

where the scalar damage functions Φ_j control the amount of growth and the vector-valued matrix q_{ij} ($i = 1, \dots, 6, j = 1, \dots, 13$) provide the coupling between the individual damage variables (i) and the various damage modes (j).

Experimental and literature sources [17] were used to obtain the material properties of the 3D woven composite, with SHPB experiments conducted for some properties and literature utilized for those without experimental data.

3.3.3 Cohesive zone model

To model the bond between Ti and the composite material, cohesive elements were utilized, specifically through the implementation of the cohesive zone method (CZM) in LS-DYNA with material_138, referred to as cohesive mixed mode. This material model employs a bilinear traction separation law for both normal and tangential directions, which are then combined to produce the mixed mode response. The model's two linear sections represent an elastic zone and a degradation zone, with the area under the curve representing the energy release rate - GIC and GIIC for the normal and tangential directions, respectively.

3.4 Finite element models

According to the experimental procedure that provided the data for model validation [6], two finite element models were constructed. The first experimental series contained single-sided shots and correspondingly acquired backface velocity measurements, using the VISAR diagnostic. The model was designed in a similar manner, wherein the complete specimen geometry was simulated in LS-DYNA explicit FE code, utilizing ELFORM 1 constant stress solid elements for the Ti and CFRP parts and ELFORM 19, 8-noded, 4-point cohesive elements for the CZM that simulates the bond. The mesh design is progressively refined towards the center, the area where the loading is applied. Subsequently, a single node located on the backface of the specimen was designated as a measuring point, where particle velocity was recorded as the simulation output. Figure 6 presents the mesh for the first FE model, highlighting the area of loading application.

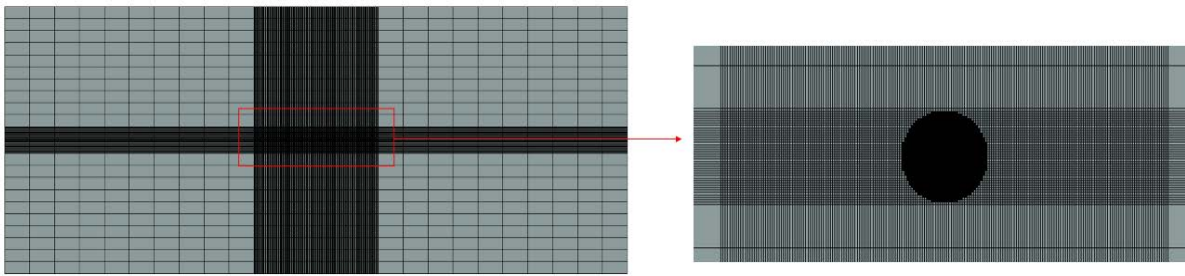


Figure 6: FE model for the single shot simulation

The second model was formulated with reference to the second experimental series, which involved conducting symmetric laser-shock experiments at the edge of the specimen for the purpose of evaluating the resultant damage. To this end, a finite element (FE) model was developed, corresponding to the first model, with a progressively refined mesh implemented towards the edge of the specimen, where successive loadings were applied. It is worth noting that the loading configuration utilized in the FE model was consistent with that employed in the experiments, whereby both surfaces of the specimen were loaded, and the bottom surface was delayed by $3.55 \mu\text{s}$. This is in accordance with the experimental procedure described in reference [7]. Figure 7 presents the mesh for the second FE model indicating the overlapping areas of load application.

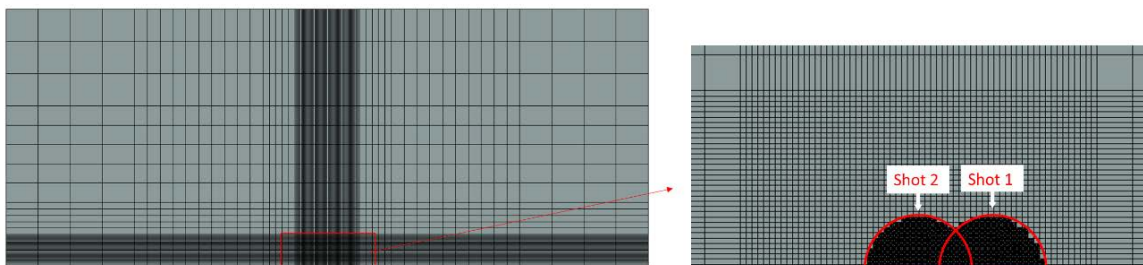


Figure 7: FE model for the symmetric simulation

3.5 Simulation procedure

To apply the laser-shock technique as a disassembly process, it is imperative to execute multiple consecutive shots, either at the same location or by moving it. This aspect is a crucial component of simulating the process, particularly for symmetric loading. Prior research [18], [19] was incorporated during the experimental procedure to induce damage at the bond line in two stages. The first load was employed to degrade the bond-line properties, while the second one caused debonding. The process is repeated using an overlapping spot to propagate the initial debonding.

To simulate this complex process, a Python script was utilized to manage and automatically execute the simulations. The script employs the Python tool qd-cae [20], which allows for keyword manipulation through Python. The code requires two keyfiles as inputs. The first keyfile is a standard LS-Dyna keyfile, with the addition of the *INTERFACE_SPRINGBACK keyword, enabling the automatic creation of a dynain binary file that contains all the simulation history variables, as well as the deformed geometry. The second keyfile is a supporting file without geometry containing the remaining information (loading spots, material properties, element formulations, etc.). The deformed geometry is provided through the dynain file, and since the element and node IDs remain unchanged, all the information of the secondary keyword is applied. The code introduces the load sequence according to the desired logic. For instance, in the case of symmetric loading simulated in this study, the loading sequence is introduced as segment set IDs. Moreover, the recursion of the code can be modified to apply a load twice at the same spot, as done in this study.

4 SIMULATION RESULTS

4.1 Single-sided shots

Numerical back-face velocity curves obtained from simulating single-sided shots can be utilized to validate the propagation of shock waves and confirm that the simulation method and material properties are an accurate representation of reality, through comparison with experimental curves. Figure 8 presents the comparison between simulation and experimental curves.

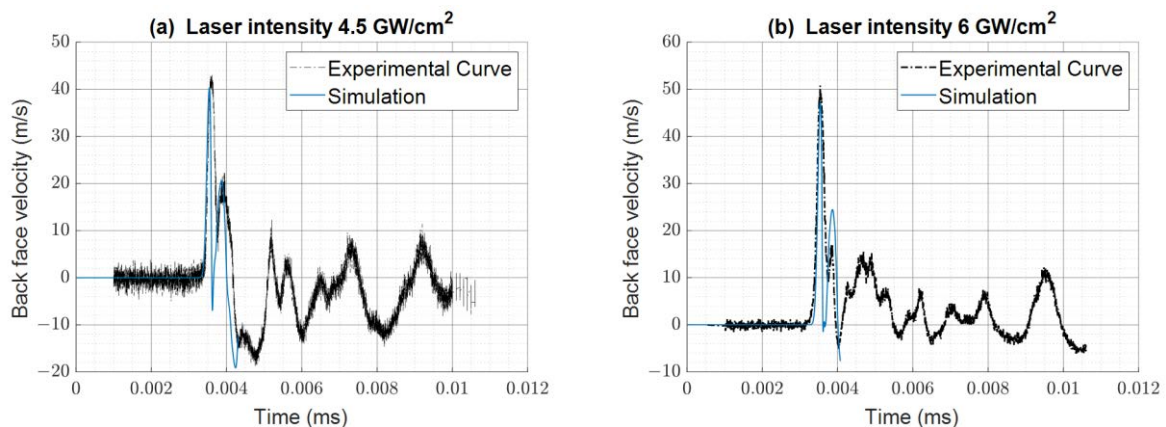


Figure 8: Simulation backface velocity against experimental data for the 4.5 GW/cm² (a) and 6 GW/cm² (b) laser intensities

The simulated backface velocity demonstrates a strong correlation with the experimental measurements, particularly at the initial peak of the curve, which is the primary focus during disassembly simulation. The observed overestimation of the release wave is attributable to heightened backface deceleration, preventing it from being reaccelerated by the succeeding shock wave.

4.2 Symmetric loading

The simulation procedure followed experimental logic for the symmetric loading, requiring two subsequent loadings at the same spot to initiate a debonding between the Ti and CFRP. The initial loading event caused bond damage, evident through plastic deformation at the shot site and the effective plastic strain history variable in the model, as presented in figure 9. Subsequently, the second loading event induced adhesive failure at the interface between the Ti and bond, ultimately leading to debonding. Cohesive element deletion captured the debonding in the simulation, given that the interface was not modeled separately, as shown in figure 10. Next, the spot was shifted by 2 mm, and the identical process was repeated, resulting in a debonding event measuring 3.9 mm in length. Following the same procedure in the simulation, the resulting cohesive element deletion measured 4.2 mm, as demonstrated in Figure 10 (b).

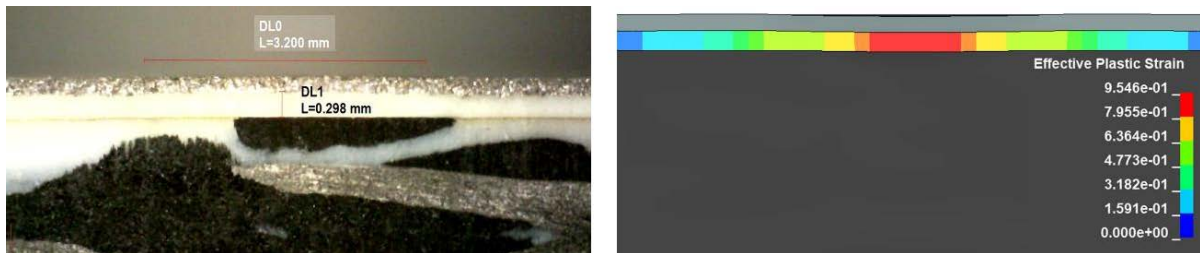


Figure 9: First shot. comparison between simulation and experiment. The Fringe result indicates the damage state of the CZM, with 0 being undamaged and upon reaching 1 the element gets deleted.

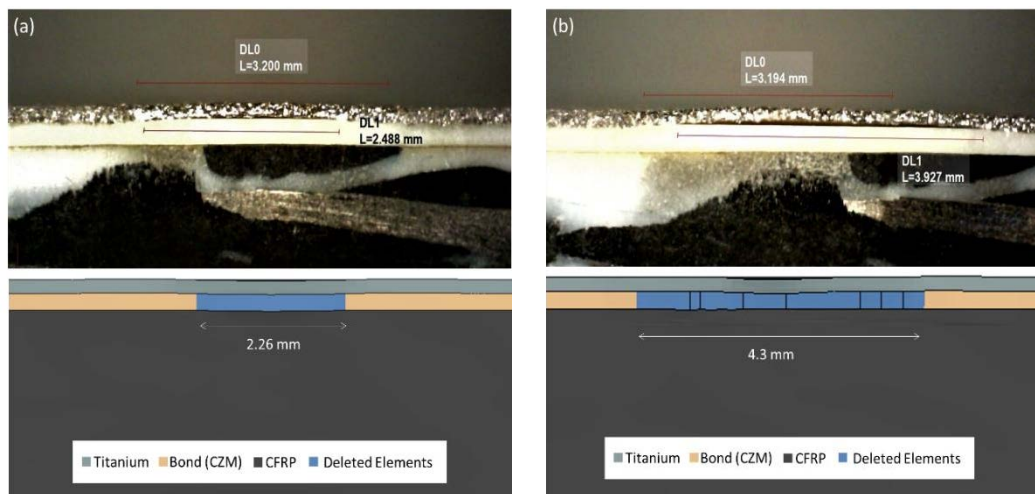


Figure 10: Damage comparison between the simulation and the experiment. After the second shot (a) and after the fourth shot (b)

It is worth mentioning that neither the experiments or the simulation resulted in any form of damage at the CFRP, meaning that the process is accurate enough to focus the tensile stress exclusively at the interface between Ti and CFRP.

5 DISCUSSION

The laser-shock technique involves complex phenomena that are sensitive to experimental parameters. The developed numerical model shows good correlation with experimental data and therefore, it becomes a valuable tool for parameter identification and process optimization. Known parameters that effect the wave propagation and the interactions between the waves that are simultaneously propagate inside the material, are the laser pulse duration as well as the delay between pulses that is applied on symmetric and double shot configurations. In additional to those, the spot diameter is a critical parameter that needs optimization. exhibits a converse correlation with the debonded area and the intensity of the lase. By increasing the spot diameter, the intensity of the laser is reduced, while decreasing it can produce very small debondings that are inefficient for a disassembly process. Thus, an optimal spot diameter should be identified based on current availability in laser technology. Furthermore, the process and the numerical model are focused on a flat geometry that simplifies study of wave propagation and its interactions. For the process to be universally utilized as a disassembly technique, it is crucial to study complex geometries such as curved panels. The model parameters are easily transferable in a curved panel simulation for further study.

6 CONCLUSIONS

The laser-shock based disassembly process for adhesively bonded structures is being simulated using the LS-Dyna explicit FE code in order to create a validated model that can be used to optimize the process. To provide accurate material properties for the 3D woven composite, high strain rate SHPB tensile and punch shear experiments where conducted. The simulation process followed the experimental procedure, where first a set of single sided experiments were held, and back-face velocity measurements were obtained. Those measurements were used as a method of comparing the numerical model to the experiment and the results correlate well for the first two peaks that are important for the process. Subsequently, symmetric laser-shock experimental results that showcase adhesive damage between the Ti and CFRP using digital microscope photographs are compared to the damage that is predicted by the CZM. The model is capable of predicting the damage area with a small deviation from the experimental data. This deviation is not affecting the method's capability to optimize the process, as absolute values of the debonding are not the main focus of the study.

Acknowledgement

The research leading to these results is part of the MORPHO project and has received funding from the European Union's Horizon 2020 research and innovation program under grant agreement No. 101006854.

REFERENCES

- [1] X. Zhao, W. J. C. Verhagen, and R. Curran, “Disposal and Recycle Economic Assessment for Aircraft and Engine End of Life Solution Evaluation,” *Applied Sciences*, vol. 10, no. 2, p. 522, Jan. 2020, doi: 10.3390/app10020522.
- [2] M. Sabaghi, Y. Cai, C. Mascle, and P. Baptiste, “Sustainability assessment of dismantling strategies for end-of-life aircraft recycling,” *Resources, Conservation and Recycling*, vol. 102, pp. 163–169, Sep. 2015, doi: 10.1016/j.resconrec.2015.08.005.
- [3] D. V. Srinivasan and S. Idapalapati, “Review of debonding techniques in adhesively bonded composite structures for sustainability,” *Sustainable Materials and Technologies*, vol. 30, p. e00345, Dec. 2021, doi: 10.1016/j.susmat.2021.e00345.
- [4] G. Piazza, M. Burczyk, M. Gerini-Romagnoli, G. Belingardi, and S. A. Nassar, “Effect of thermally expandable particle additives on the mechanical and reversibility performance of adhesive joints,” *Journal of Advanced Joining Processes*, vol. 5, p. 100088, Jun. 2022, doi: 10.1016/j.jajp.2021.100088.
- [5] M. D. Banea, “Debonding on Demand of Adhesively Bonded Joints: A Critical Review,” *rev adhesives*, vol. 7, no. 1, pp. 33–50, Mar. 2019, doi: 10.7569/RAA.2019.097304.
- [6] P. Kormpos, S. Unaldi, L. Berthe, and K. Tserpes, “A Laser Shock-Based Disassembly Process for Adhesively Bonded Ti/CFRP Parts,” *Processes*, vol. 11, no. 2, p. 506, Feb. 2023, doi: 10.3390/pr11020506.
- [7] K. Papadopoulos and K. Tserpes, “Analytical and Numerical Modeling of Stress Field and Fracture in Aluminum/Epoxy Interface Subjected to Laser Shock Wave: Application to Paint Stripping,” *Materials*, vol. 15, no. 10, p. 3423, May 2022, doi: 10.3390/ma15103423.
- [8] K. Tserpes, K. Papadopoulos, S. Unaldi, and L. Berthe, “Development of a Numerical Model to Simulate Laser-Shock Paint Stripping on Aluminum Substrates,” *Aerospace*, vol. 8, no. 9, p. 233, Aug. 2021, doi: 10.3390/aerospace8090233.
- [9] S. Unaldi *et al.*, “Towards selective laser paint stripping using shock waves produced by laser-plasma interaction for aeronautical applications on AA 2024 based substrates,” *Optics & Laser Technology*, vol. 141, p. 107095, Sep. 2021, doi: 10.1016/j.optlastec.2021.107095.
- [10] R. Ecault, F. Touchard, M. Boustie, L. Berthe, and N. Dominguez, “Numerical modeling of laser-induced shock experiments for the development of the adhesion test for bonded composite materials,” *Composite Structures*, vol. 152, pp. 382–394, Sep. 2016, doi: 10.1016/j.compstruct.2016.05.032.
- [11] H. Huh, W. J. Kang, and S. S. Han, “A tension split Hopkinson bar for investigating the dynamic behavior of sheet metals,” *Experimental Mechanics*, vol. 42, no. 1, pp. 8–17, Mar. 2002, doi: 10.1007/BF02411046.
- [12] M. V. Hosur, S. M. W. Islam, U. K. Vaidya, P. K. Dutta, and S. Jeelani, “Experimental studies on the punch shear characterization of satin weave graphite/epoxy composites at room and elevated temperatures,” *Materials Science and Engineering: A*, vol. 368, no. 1–2, pp. 269–279, Mar. 2004, doi: 10.1016/j.msea.2003.11.001.
- [13] R. Fabbro, P. Peyre, L. Berthe, and X. Scherpereel, “Physics and applications of laser-shock processing,” *Journal of Laser Applications*, vol. 10, no. 6, pp. 265–279, Dec. 1998, doi: 10.2351/1.521861.
- [14] “LS-DYNA Keyword user’s manual, LS-DYNA R11, Volume I, II, III, Livermore Software Technology Corporation (LSTC).”
- [15] J. Chen, W. Chen, S. Chen, G. Zhou, and T. Zhang, “Shock Hugoniot and Mie-Grüneisen EOS of TiAl alloy: A molecular dynamics approach,” *Computational Materials Science*, vol. 174, p. 109495, Mar. 2020, doi: 10.1016/j.commatsci.2019.109495.
- [16] Y. Zhang, J. C. Outeiro, and T. Mabrouki, “On the Selection of Johnson-cook Constitutive Model Parameters for Ti-6Al-4V Using Three Types of Numerical Models of Orthogonal Cutting,” *Procedia CIRP*, vol. 31, pp. 112–117, 2015, doi: 10.1016/j.procir.2015.03.052.
- [17] M. Tehrani, A. Yari Boroujeni, and M. Al-Haik, *Modeling and simulation of impact and perforation in fiber reinforced composites*. 2014.
- [18] P. Kormpos, K. Tserpes, and G. Floros, “Towards simulation of disassembly of bonded composite parts using the laser shock technique.,” *IOP Conference Series: Materials Science and Engineering*, vol. 1226, no. 1, p. 012081, Jan. 2022.
- [19] P. Kormpos, S. Unaldi, M. Ayad, L. Berthe, and K. Tserpes, “Towards the development of a laser shock-based disassembly process for adhesively bonded structural parts: Experiments and numerical simulation,” *Proceedings of the 20th European Conference on Composite Materials - Composites Meet Sustainability*, vol. B, pp. 873–880, doi: 10.5075/epfl-298799_978-2-9701614-0-0.
- [20] C. Diez, “qd-cae.” 2018. [Online]. Available: <https://github.com/qd-cae>